

Supporting Information for

Rapid and Accurate Estimation of Protein-Ligand Relative Binding Affinities using the Site-Identification by Ligand Competitive Saturation Approach

Himanshu Goel,^{1†} Anthony Hazel,^{1†} Vincent D. Ustach,¹ Sunhwan Jo,² Wenbo
Yu,¹ and Alexander D. MacKerell Jr.^{1,2*}

¹ Department of Pharmaceutical Sciences, University of Maryland School of Pharmacy, 20 Penn
Street, HSF II, Baltimore, Maryland 21201, United States

² SilcsBio LLC, 8 Market Place, Suite 300, Baltimore, MD 21202, United States

[†] These authors equally contributed to this work.

Table of Contents

Metrics for Comparing the Calculated and Experimental Relative Binding Affinities	3
Atom Classification Schemes (ACS)	4
Calculation of Experimental Binding Free Energies	7
Tables	8
<i>Table S1: SILCS-MC GFE scaling parameters for SILCS 2021 ACS</i>	8
<i>Table S2: Ligand placement centers</i>	9
<i>Table S3: Overlap coefficients for standard SILCS</i>	10
<i>Table S4: Overlap coefficients for halogen SILCS-X</i>	11
<i>Table S5: Performance of SILCS 2018 ACS</i>	12
<i>Table S6: Performance of SILCS PC-based ML-optimization for 199 ligands</i>	13
<i>Table S7: Overall performance for 330 ligand perturbations</i>	15
<i>Table S8: Individual protein target performances for 330 ligand perturbations</i>	16
<i>Table S9: Performance of SILCS PC-based ML-optimization for 407 ligands</i>	17
Figures	19
<i>Figure S1: SILCS workflow</i>	19
<i>Figure S2: SILCS and SILCS-X solutes</i>	20
<i>Figure S3: Experimental ΔG's</i>	21
<i>Figure S4: Correlation plots of raw LGFE Scores for 199 ligands</i>	22
<i>Figure S5: Correlation plots of computed SILCS ΔG's for 199 ligands</i>	23
<i>Figure S6: Standard deviations of computed SILCS ΔG's for 199 ligands</i>	24
<i>Figure S7: Standard deviations of SILCS MUE scores for 199 ligands</i>	25
<i>Figure S8: Standard deviations of SILCS PC scores for 199 ligands</i>	26
<i>Figure S9: Correlation plots of computed SILCS PC-based ML-optimized ΔG's for 199 ligands</i>	27
<i>Figure S10: Outlier ligands of P38</i>	28
<i>Figure S11: Correlation plots of computed $\Delta\Delta G$'s for 330 ligand perturbations</i>	29
<i>Figure S12: Error distributions of computed $\Delta\Delta G$'s for 330 ligand perturbations</i>	30

<i>Figure S13: Error distributions of computed ΔG's for 407 ligands</i>	31
<i>Figure S14: Correlation plots of computed SILCS ΔG's for 407 ligands</i>	32
<i>Figure S15: Correlation plots of computed SILCS PC-based ML-optimized ΔG's for 407 ligands</i>	33
<i>Figure S16: Atom classifications for two representative ligands</i>	34
References	35

Metrics for Comparing the Calculated and Experimental Relative Binding Affinities

Comparison of the SILCS-MC relative affinities with experimental data were performed based on the metrics of predictive index (PI), percent correct (PC), Pearson's correlation coefficient (R), root mean square error (RMSE), and mean unsigned error (MUE). PC is the number of correct predictions of all the ligands with respect to the reference ligand based on direction of the change in the binding free energy divided by the total number of ligands. Note that if two ligands have the same experimental binding free energy but different computed binding free energies, then their comparison results in one true negative and one false positive.* The reported PC values represent the average over all individual PC values for each ligand being considered as the reference ligand. A PC values of 1 indicates optimal binding order prediction. The PI correlation varies between 1 for 100 % true relative predictions and -1 for 100 % false predictions, and 0 for random predictions. It can also be defined as a metric to rank the order of ligands based on their affinities. R is the Pearson correlation and varies between -1 to 1, with 1 denoting perfectly correlated data and -1 denoting perfectly anti-correlated data. MUE and RMSE denote the average absolute difference and the root mean square difference, respectively, between the calculated and experimental relative binding affinities values. Formulas for calculating all performance metrics are given in SI files si_199.xlsm and si_407.xlsm.

* For example, ligand A and ligand B have the same experimental binding affinity, but different computed binding affinities. When calculating PC, we have to compare A to B, and then B to A. Since a comparison can only be positive if one binding affinity is lower than the other, both comparisons are considered to be negatives as the ligands have the same experimental binding affinity. But since they have different computed binding affinities, one of the comparisons will be positive and the other negative. Thus, we have two experimental negatives and one computational positive and negative. This results in one true negative (both experimental and computational comparisons are negative) and one false positive (experimental negative but computational positive). Therefore, the average contribution of comparing these two ligands is 0.5, with one true result (value of 1) and one false result (value of 0). For predictive index, these comparisons would be given a weight of 0 (between -1 and 1), yielding a similar result.

Atom Classification Schemes (ACS)

SILCS ligand binding affinity estimates are based on the FragMap GFE values for each grid point that a particular atom overlaps, requiring each atom in a ligand be assigned to one of the FragMap types or be assigned as not classified (NCLA). NCLA types include all hydrogens and selected non-hydrogen atoms, such as carbons adjacent to polar functional groups such as that in methanol. NCLA-classified atoms are assigned a GFE score of 0. The GFE scores for the individual atoms are then summed to yield the ligand GFE (LGFE) which is the SILCS estimate of the ligand binding affinity. As described in the main text, LGFE is not a true binding affinity. For this study, we employed two atom classification schemes (ACS), the 2018 ACS, which has been extensively tested in a previous SILCS study,¹ and the new 2021 ACS. For the 2018 ACS, the GFE values from FragMaps calculated using multiple solute atoms (e.g. 6 carbons in benzene) were inversely scaled by their respective atom counts during SILCS-MC. This was done to avoid overcounting, which tended to produce too favorable LGFE scores for the 2016 ACS employed previously.^{1,2} This additional scaling also helps to directly map SILCS fragments to ligand fragments; e.g. the six benzene carbons used to calculate the BENC FragMap are directly mapped to six aromatic carbons within a ligand. Other changes for the 2018 ACS involve classification of larger charged groups, such as phosphates and sulfates, and atoms adjacent to functional groups. For the 2021 ACS, we have replaced the acetaldehyde (AALD) solute in the standard set of SILCS solutes with the dimethylether (DMEE) solute, which is also present in the halogen set of SILCS solutes. As formamide (FORM) is also in the standard set of SILCS solutes, replacing AALD with DMEE reduces redundancies in the FragMaps and allows for more diverse chemical classifications with just the standard set alone. When present, the standard DMEE fragment is used to calculate all DMEE-based FragMaps, while the halogen DMEE fragment is ignored. Methanol is treated in a similar fashion.

Similar atom types are combined to create “generic” FragMaps that can be applied more broadly than their “specific” counterparts. These are detailed as follows: the generic non-polar (GENN) or apolar FragMaps are based on the benzene and propane carbons; the generic heterocyclic (GEHC) atom type from imidazole carbons; the generic donor (GEND) atom type from formamide nitrogen and protonated imidazole nitrogen; and the generic acceptor (GENA) atom type from formamide

oxygen, un-protonated imidazole nitrogen, and either acetaldehyde oxygen (2018 ACS) or dimethylether oxygen (2021 ACS). Methanol oxygens and aldehydic carbons can act as both donors and acceptors, so they are treated explicitly with the methanol oxygen (MEOO) atom type and either the acetaldehyde carbon (AALC, 2018 ACS) or formamide carbon (FORC, 2021 ACS) atom type, respectively. For charged functional groups we also include a methylammonium nitrogen (MAMN) atom type for positively charged groups, and an acetate carbon (ACEC) atom type for negatively charged groups. For standard SILCS-MC, halogens are treated as GENA based on previous work from our lab indicating favorable interactions with hydrogen bond donors,³ with the exception of TFEC and the aliphatic chlorine- and bromine-containing groups which are treated using PRPC.

Several atom types are common to all atomic scaling schemes. These include GENN, GEHC, GEND, GENA, ACEC, MAMN, MEOO and either AALC (2018 ACS) or FORC (2021 ACS). BENC and PRPC are also common atom types, although, as discussed below, they are treated differently in Generic and Specific schemes. MEOO type is used to explicitly treat hydroxyl groups in all schemes due to these groups acting as both hydrogen bond donors and acceptors. As discussed above, additional scaling of the GFE values during SILCS-MC is done to properly impose solute-to-atom mapping from FragMap GFEs to SILCS-MC GFEs. For this work, we have removed this additional SILCS-MC GFE scaling for the GEND and GENA atom types (see Table S1), as, for these atom types, the FragMaps are often only mapped to a single atom during SILCS-MC so no additional scaling is required.

Generic Apolar Scale 2018 and 2021 (GAS18 and GAS21): Benzene carbon (BENC) and propane carbon (PRPC) atom types utilize the generic nonpolar map (GENN) with SILCS-MC GFE scaling of 0.167 and 0.333, respectively.

Specific Standard 2018 and 2021 (SS18 and SS21): Specific maps are used for most atom types, with some generic maps also being utilized such as GEHC for heterocyclic carbons. For SS18, ether and furan oxygens are treated as GENA, while for SS21 they are treated explicitly as DMEO. Specific atom types include benzene carbon (BENC), propane carbon (PRPC), formamide nitrogen (FORN), formamide oxygen (FORO), formamide carbon (FORC, SS21 only), acetaldehyde

oxygen (AALO, SS18 only), acetaldehyde carbon (AALC, SS18 only), imidazole unprotonated nitrogen (IMIN), and imidazole protonated nitrogen (IMIHI). Note that for the specific scaling, BENC and PRPC do not use the GENN map as was the case for the Generic scaling. When AALC or FORC is used to represent aldehydes as both donors and acceptors, the corresponding oxygen atoms are set to NCLA.

Halogen Maps (GAX18, SX18, GAX21, and SX21): The SILCS halogen set, “SILCS-X”, includes maps for fluoroethane fluorine (FETX), trifluoroethane carbon (TFEC), fluorobenzene fluorine (FLBX), chloroethane chlorine (CLEX), chlorobenzene chlorine (CLBX), and bromobenzene bromine (BRBX). Trifluoromethyl groups are treated based on the trifluoroethane carbon (TFEC), while in trichloro- and tribromomethyl groups the carbons are NCLA and the contribution is based on the aliphatic chlorine (CLEX). The SILCS-X set is also supplemented with dimethylether and methanol fragments. GAX18 and SX18 use the dimethylether fragment in the SILCS-X set to calculate the dimethylether oxygen (DMEO) FragMaps. For GAS21 and SX21, DMEO FragMaps are calculated from the standard SILCS set, which now includes dimethylether fragments as detailed above.

Calculation of Experimental Binding Free Energies

We have recalculated the experimental binding affinities using the reported K_i or IC_{50} values for each ligand from their respective sources using equations 1.4 and 1.5 from the Supplemental Information of Wang et al.⁴ For ligands reported as racemic mixtures, or those with chiral center for which an enantiomer was not specified, the reported K_i or IC_{50} values were divided by 2, as specified by Wang et al.⁴ Our reported experimental binding free energies for the 199 ligand set match those of Wang et al.⁴ except in the case of Thrombin. For Thrombin, isothermal titration calorimetry (ITC) was used to calculate absolute binding free energies, ΔG , for a subset of 11 ligands in the original experimental work by Baum et al.⁵, in addition to determining kinetic inhibition constants, K_i , for all 26 ligands in that study. Wang et al.⁴ used these 11 ITC ligands with their respective ΔG values instead of converting their reported K_i values to ΔG 's. Because we intend to also test the remaining 17 ligands for which ITC was not performed, we did not use the ΔG values for those 11 ITC ligands, instead converting K_i values to ΔG 's for all ligands. Differences in our calculated experimental ΔG 's and those reported used in Wang et al.⁴ for the Thrombin ligands are shown in Figure S3. There is an overall correlation of $R = 0.89$ and MUE of 0.427 kcal/mol between the two sets of experimental results for the 11 ITC ligands (see Figure S3). For transparency, we have included both experimental K_i/IC_{50} and binding free energy values in files `si_199.xlsm` and `si_407.xlsm`. Due to the aforementioned discrepancies, we have readjusted the results from Wang et al.⁴ Song et al.⁶ Gapsys et al.⁷ and Kuhn et al.⁸ using our recalculated experimental binding affinities. All results and analysis reported in this study utilize these readjusted binding affinities. We note that with our corrected experimental data, some of the methods perform better for individual protein targets than reported in their original works, while others perform worse than reported. For example, Wang et al.⁴ reported an MUE of 0.76 kcal/mol for Thrombin, while we computed a lower MUE of 0.47 kcal/mol for their data set, but with R^2 unchanged. Conversely, Kuhn et al.⁸ reported an MUE of ~ 0.20 kcal/mol and a R^2 of ~ 0.82 for Thrombin, while we computed a higher MUE of 0.57 kcal/mol and a lower R^2 of 0.56 for their data set. Our corrected experimental data either improved or did not affect the overall performance of the reported methods, with the exception of the Kuhn et al.⁸ study, which exhibited a slight decrease in correlation.

Table S1: SILCS-MC GFE scaling parameters for 2021 ACS.

^aCombination of forn and iminh FragMaps. ^bCombination of foro, dmeo, and imin FragMaps.

^cCombination of benc and prpc FragMaps; for GAS21 and GAX21, only. ^dAtom type not used.

Atom type	FragMap	Weights			
		GAS21	GAX21	SS21	SX21
GEND	hbdon ^a	1.000	1.000	1.000	1.000
GENA	hbacc ^b	1.000	1.000	1.000	1.000
BENC	apolar ^c /benc	0.167	0.167	0.167	0.167
PRPC	apolar ^c /prpc	0.333	0.333	0.333	0.333
MEOO	meoo	1.000	1.000	1.000	1.000
FORC	forc	1.000	1.000	1.000	1.000
FORN	forn	- ^d	-	1.000	1.000
FORO	foro	-	-	1.000	1.000
DMEO	dmeo	-	-	1.000	1.000
IMIN	imin	-	-	1.000	1.000
IMIH	iminh	-	-	1.000	1.000
GEHC	gehc	0.333	0.333	0.333	0.333
MAMC	mamn	1.000	1.000	1.000	1.000
MAMN	mamn	1.000	1.000	1.000	1.000
ACEC	acec	1.000	1.000	1.000	1.000
FETX	fetx	-	1.000	-	1.000
FTEC	tfec	-	1.000	-	1.000
CLEX	clcx	-	1.000	-	1.000
FLBX	flbx	-	1.000	-	1.000
CLBX	clbx	-	1.000	-	1.000
BRBX	brbx	-	1.000	-	1.000

Table S2: Ligand placement centers for all eight protein targets. Coordinates are relative to the given PDB structures.

Target	PDB	X (Å)	Y (Å)	Z (Å)
P38	3FLY	34.950	28.150	36.970
BACE	4DJW	21.784	10.981	21.468
MCL1	4HW3	37.061	20.757	28.654
TYK2	4GIH	31.290	32.110	35.920
JNK1	2GMX	21.272	66.977	8.246
Thrombin	2ZFF	17.257	-12.722	22.438
CDK2	1H1Q	-5.723	22.716	-22.687
PTP1B	2QBS	47.625	10.960	2.318

Table S3: Overlap coefficient from simulation sets 1-5 and 6-10 for the different solute atom types as well as water oxygens in the standard SILCS simulations for each protein target.

Target 	P38	BACE	MCL1	TYK2	JNK1	Thrombin	CDK2	PTP1B
Solute 								
Dimethylether oxygen (dmeo)	0.81	0.82	0.79	0.81	0.81	0.81	0.82	0.80
Methanol oxygen (meoo)	0.82	0.83	0.80	0.82	0.82	0.81	0.82	0.82
Imidazole acceptor nitrogen (imin)	0.80	0.79	0.81	0.80	0.80	0.80	0.80	0.80
Imidazole donor nitrogen (iminh)	0.80	0.79	0.80	0.80	0.80	0.79	0.79	0.80
Formamide oxygen (foro)	0.82	0.82	0.81	0.81	0.82	0.81	0.82	0.82
Formamide nitrogen (forn)	0.82	0.82	0.81	0.81	0.82	0.81	0.82	0.82
Formamide carbon (forc)	0.82	0.82	0.81	0.81	0.82	0.81	0.82	0.82
Methylammonium nitrogen (mamn)	0.80	0.80	0.77	0.78	0.80	0.77	0.79	0.78
Acetate carbon (acec)	0.75	0.76	0.75	0.75	0.76	0.75	0.76	0.72
Benzene carbon (benc)	0.88	0.90	0.87	0.88	0.88	0.89	0.89	0.87
Propane carbon (prpc)	0.85	0.86	0.83	0.85	0.85	0.85	0.85	0.84
Imidazole carbon (gehc)	0.87	0.87	0.87	0.87	0.87	0.87	0.87	0.87
Average	0.82	0.82	0.81	0.82	0.82	0.81	0.82	0.81
Water oxygen (tipo)	0.97	0.97	0.97	0.97	0.97	0.97	0.97	0.97

Table S4: Overlap coefficient from simulation sets 1-5 and 6-10 for the different solute atom types as well as water oxygens in the halogen SILCS-X simulations for each protein target.

Target →	P38	BACE	MCL1	TYK2	JNK1	Thrombin	CDK2	PTP1B
Solute ↓								
Bromobenzene bromine (brbx)	0.72	0.75	0.77	0.77	0.73	0.70	0.74	0.70
Chlorobenzene chlorine (clbx)	0.71	0.75	0.77	0.78	0.72	0.70	0.73	0.69
Fluorobenzene fluorine (flbx)	0.78	0.80	0.78	0.78	0.79	0.78	0.79	0.78
Chloroethane chlorine (clex)	0.78	0.79	0.77	0.77	0.77	0.78	0.78	0.77
Fluoroethane fluorine (fetx)	0.77	0.82	0.77	0.77	0.78	0.75	0.78	0.76
Trifluoroethane carbon (tfec)	0.78	0.80	0.77	0.78	0.78	0.78	0.79	0.78
Average	0.76	0.79	0.77	0.78	0.76	0.75	0.77	0.75
Water oxygen (tipO)	0.97	0.99	0.97	0.97	0.97	0.97	0.97	0.97

Table S5: Average metrics over all eight protein targets using the SILCS 2018 ACS. r_{LP} is the ligand placement radius. MUE/RMSE values in units of kcal/mol.

Protocol (radius)	ACS	MUE	RMSE	R	PI	PC
Exhaustive ($r_{LP} = 5 \text{ \AA}$)	GAS18	0.814	0.995	0.437	0.444	0.657
Exhaustive ($r_{LP} = 5 \text{ \AA}$)	GAX18	0.903	1.096	0.401	0.426	0.638
Exhaustive ($r_{LP} = 5 \text{ \AA}$)	SS18	0.755	0.917	0.532	0.517	0.687
Exhaustive ($r_{LP} = 5 \text{ \AA}$)	SX18	0.919	1.149	0.425	0.450	0.653
Difference: 2021 ACS - 2018 ACS						
Exhaustive ($r_{LP} = 5 \text{ \AA}$)	GAS18	-0.013	0.016	0.018	0.015	0.003
Exhaustive ($r_{LP} = 5 \text{ \AA}$)	GAX18	-0.075	-0.059	0.132	0.103	0.045
Exhaustive ($r_{LP} = 5 \text{ \AA}$)	SS18	0.062	0.118	-0.059	-0.029	-0.010
Exhaustive ($r_{LP} = 5 \text{ \AA}$)	SX18	-0.119	-0.135	0.189	0.190	0.066

Table S6: Metrics obtained from the SILCS PC-based ML optimization procedure with all the ACS with a ligand placement radius of 5 Å for 199 ligands.

Method	System	MUE	RMSE	R	PI	PC
GAS21*-5 Å (199 ligands)	P38	0.802	1.030	0.528	0.572	0.709
	BACE	0.542	0.763	0.536	0.666	0.724
	MCL1	0.663	0.829	0.631	0.645	0.737
	TYK2	0.995	1.196	0.315	0.471	0.642
	JNK1	0.676	0.821	0.706	0.730	0.812
	Thrombin	0.672	0.795	0.600	0.828	0.818
	CDK2	0.756	0.952	0.631	0.753	0.767
	PTP1B	0.497	0.790	0.789	0.846	0.836
Average		0.700	0.897	0.592	0.689	0.756
GAX21*-5 Å (199 ligands)	P38	0.774	0.975	0.632	0.670	0.742
	BACE	1.472	1.876	0.571	0.612	0.702
	MCL1	0.848	1.049	0.721	0.745	0.776
	TYK2	0.807	0.928	0.684	0.743	0.742
	JNK1	0.607	0.769	0.686	0.698	0.788
	Thrombin	1.177	1.317	0.913	0.963	0.945
	CDK2	0.540	0.630	0.864	0.873	0.825
	PTP1B	0.623	0.867	0.739	0.839	0.840
Average		0.856	1.051	0.726	0.768	0.795
SS21*-5 Å (199 ligands)	P38	0.967	1.259	0.607	0.685	0.774
	BACE	0.536	0.753	0.563	0.673	0.733
	MCL1	0.776	0.944	0.782	0.790	0.792
	TYK2	1.063	1.235	0.251	0.247	0.550
	JNK1	0.418	0.599	0.715	0.698	0.798

	Thrombin	0.547	0.596	0.747	0.892	0.855
	CDK2	2.127	2.421	0.906	0.914	0.858
	PTP1B	0.506	0.727	0.825	0.877	0.852
Average		0.868	1.067	0.674	0.722	0.776
SX21*-5 Å (199 ligands)	P38	0.921	1.103	0.744	0.755	0.781
	BACE	0.617	0.819	0.597	0.601	0.700
	MCL1	0.685	0.802	0.761	0.743	0.778
	TYK2	0.868	1.077	0.526	0.540	0.700
	JNK1	0.905	1.171	0.723	0.688	0.764
	Thrombin	0.509	0.555	0.915	0.963	0.945
	CDK2	2.420	2.568	0.860	0.900	0.850
	PTP1B	0.622	0.724	0.865	0.944	0.895
Average		0.943	1.102	0.749	0.767	0.802

Table S7: Comparison of the total $\Delta\Delta G$ MUE and RMSE scores for the 330 perturbations used in the cycle-closure correction with respect to Wang et al. (FEP+/OPLS2.1),⁴ Song et al. (AMBER/ff14SB+GAFF1.8),⁶ Gapsys et al. (pmx GAFF/CGenFF/Consensus),⁷ and Kuhn et al. (Flare FEP/ff14SB+GAFF2.1).⁸ The MUE and RMSE are given in units of kcal/mol.

Method	MUE	RMSE
SILCS-Default SX21-5 Å	1.085	1.368
SILCS-Best PC	1.065	1.351
SILCS ML-Optimized	0.864	1.079
FEP+/OPLS 2.1	0.899	1.146
AMBER/ff14SB+GAFF1.8	1.180	1.503
Flare FEP/ff14SB+GAFF2.1	1.101	1.427
pmx GAFF2.1	0.871	1.130
pmx CGenFF	1.097	1.441
pmx Consensus	0.855	1.139

Table S8: Comparison of the relative binding affinities across 330 perturbations of the ligands for the individual protein targets. The MUE and RMSE are given in units of kcal/mol.

System	P38	BACE	MCL1	TYK2	JNK1	Thrombin	CDK2	PTP1B	Overall
Number of ligands	11	16	21	16	23	36	42	34	199
Number of perturbations	16	24	31	25	49	58	71	56	330
MUE (SILCS-Default SX21-5 Å)	1.524	0.751	1.156	0.880	1.390	0.571	0.929	1.030	1.085
RMSE (SILCS- Default SX21-5 Å)	1.717	0.960	1.409	1.116	1.709	0.692	1.178	1.397	1.368
MUE (SILCS-Best PC)	1.726	0.766	1.207	0.880	0.947	0.493	0.875	0.907	1.065
RMSE (SILCS-Best PC)	1.977	0.989	1.418	1.116	1.182	0.585	1.066	1.248	1.351
MUE (SILCS PC-Optimized)	1.199	0.703	0.818	0.844	0.984	0.627	0.698	0.833	0.864
RMSE (SILCS PC-Optimized)	1.395	0.930	1.018	1.000	1.287	0.778	0.795	1.019	1.079
MUE (FEP+/OPLS 2.1)	0.804	0.827	1.154	0.751	0.785	0.772	0.911	0.893	0.899
RMSE (FEP+/OPLS 2.1)	1.029	1.042	1.412	0.934	0.996	0.917	1.114	1.223	1.146
MUE (AMBER GPU-TI)	1.200	1.198	1.516	1.076	1.068	0.604	0.968	1.064	1.180
RMSE (AMBER GPU-TI)	1.562	1.502	1.833	1.268	1.452	0.699	1.125	1.400	1.503
MUE (Flare FEP)	1.115	1.101	1.494	0.889	0.925	0.898	1.045	0.829	1.101
RMSE (Flare FEP)	1.549	1.388	1.870	1.101	1.137	1.081	1.224	1.033	1.427
MUE (PMX GAFF)	0.698	0.834	1.243	1.017	0.739	0.704	0.722	0.713	0.871
RMSE (PMX GAFF)	0.833	1.089	1.554	1.255	0.990	0.882	0.902	0.919	1.130
MUE (PMX CGenFF)	1.086	1.027	1.586	1.185	0.723	1.145	0.864	0.778	1.097
RMSE (PMX CGenFF)	1.386	1.294	1.932	1.473	0.942	1.477	1.071	1.218	1.441
MUE (PMX Consensus)	0.715	0.873	1.251	1.012	0.430	0.709	0.744	0.718	0.855
RMSE (PMX Consensus)	0.906	1.100	1.546	1.310	0.579	0.848	0.950	1.076	1.139

Table S9: Average metrics obtained from the SILCS PC-based ML optimization procedure with all the ACS with a ligand placement radius of 5 Å for 407 ligands.

Method	System	MUE	RMSE	R	PI	PC
GAS21*-5 Å (407 ligands)	P38	0.745	0.916	0.555	0.579	0.703
	BACE	0.741	1.055	0.556	0.697	0.740
	MCL1	0.911	1.105	0.826	0.834	0.823
	TYK2	1.120	1.308	0.615	0.708	0.721
	JNK1	1.222	1.517	0.695	0.708	0.760
	Thrombin	0.903	1.159	0.640	0.665	0.715
	CDK2	0.707	0.818	0.730	0.749	0.762
	PTP1B	0.903	1.067	0.815	0.831	0.810
Average		0.906	1.118	0.679	0.721	0.754
GAX21*-5 Å (407 ligands)	P38	0.793	1.005	0.638	0.683	0.746
	BACE	1.371	1.864	0.602	0.703	0.744
	MCL1	0.624	0.767	0.887	0.886	0.858
	TYK2	1.844	2.677	0.640	0.736	0.747
	JNK1	1.076	1.408	0.731	0.741	0.782
	Thrombin	0.923	1.133	0.816	0.854	0.838
	CDK2	0.605	0.759	0.791	0.814	0.810
	PTP1B	1.438	2.283	0.580	0.817	0.806
Average		1.084	1.487	0.711	0.779	0.791
SS21*-5 Å (407 ligands)	P38	0.910	1.162	0.618	0.658	0.739
	BACE	0.559	0.815	0.658	0.761	0.773
	MCL1	0.779	0.952	0.858	0.879	0.855
	TYK2	1.548	1.941	0.655	0.658	0.717
	JNK1	1.124	1.576	0.701	0.737	0.774

	Thrombin	2.406	2.750	0.770	0.837	0.814
	CDK2	0.697	0.878	0.722	0.724	0.760
	PTP1B	1.272	1.634	0.829	0.815	0.807
Average		1.162	1.464	0.726	0.759	0.780
SX21*-5 Å (407 ligands)	P38	1.089	1.340	0.661	0.687	0.758
	BACE	0.701	1.036	0.568	0.701	0.746
	MCL1	0.913	1.126	0.886	0.892	0.859
	TYK2	0.886	1.071	0.762	0.807	0.777
	JNK1	1.236	1.575	0.706	0.733	0.771
	Thrombin	1.365	1.677	0.799	0.836	0.826
	CDK2	1.016	1.267	0.696	0.706	0.765
	PTP1B	1.097	1.405	0.808	0.803	0.805
Average		1.038	1.312	0.736	0.771	0.788

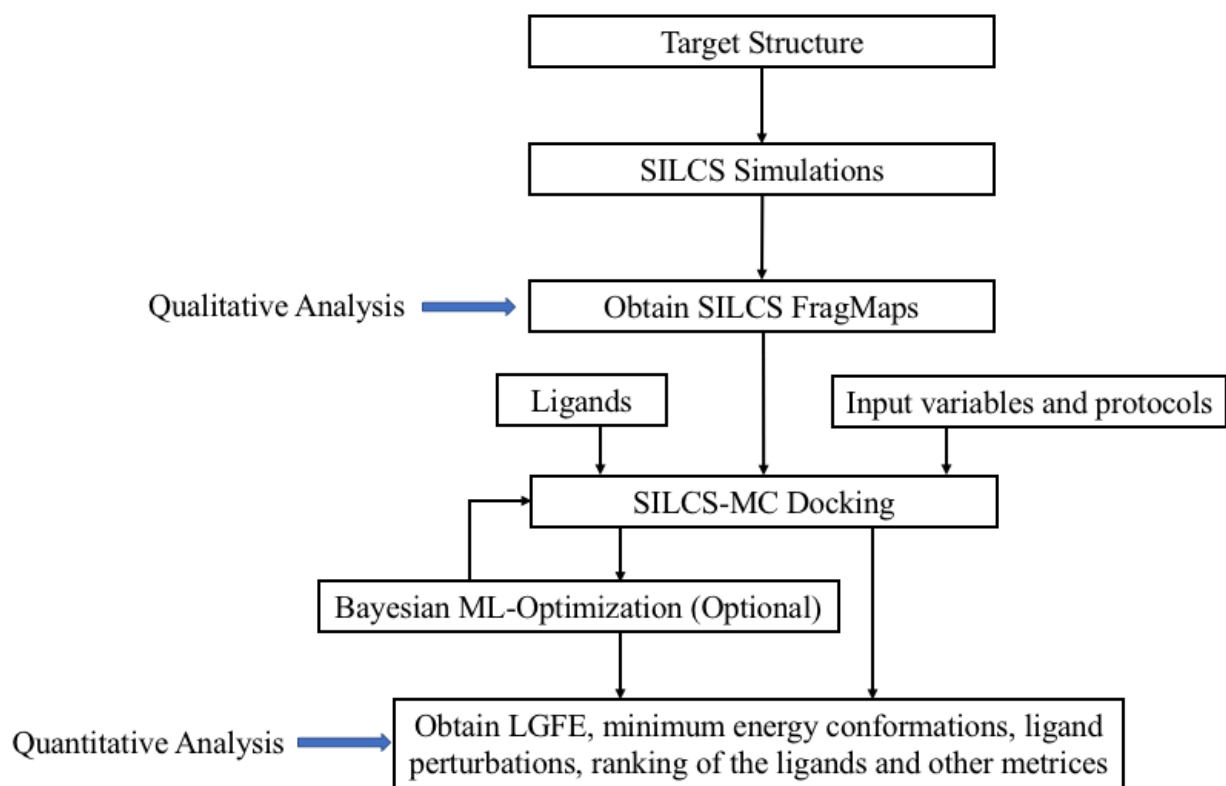


Figure S1: Flow diagram for the entire SILCS workflow.

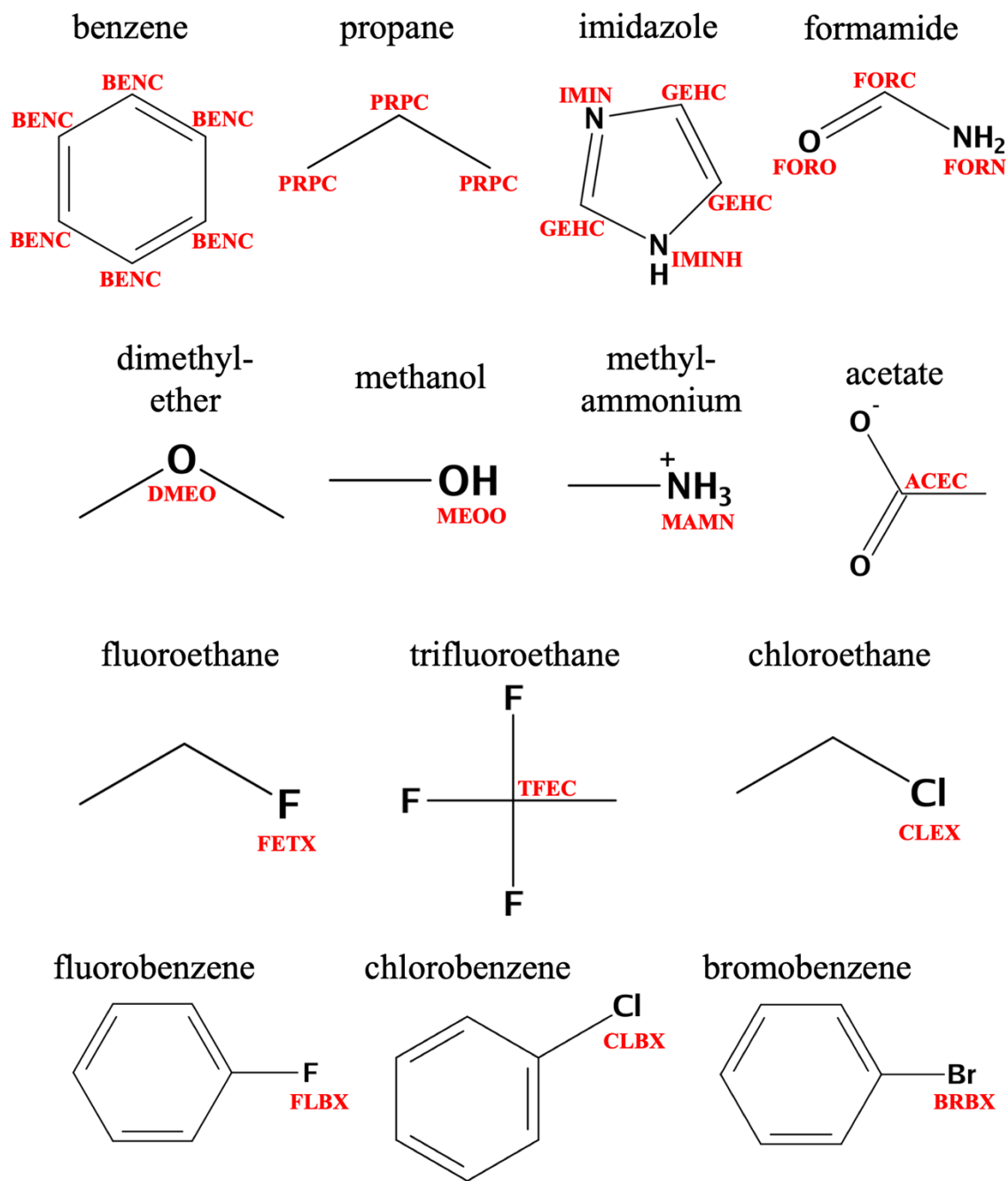


Figure S2: Solutes used for the SILCS methodologies and their corresponding FragMap atom types.

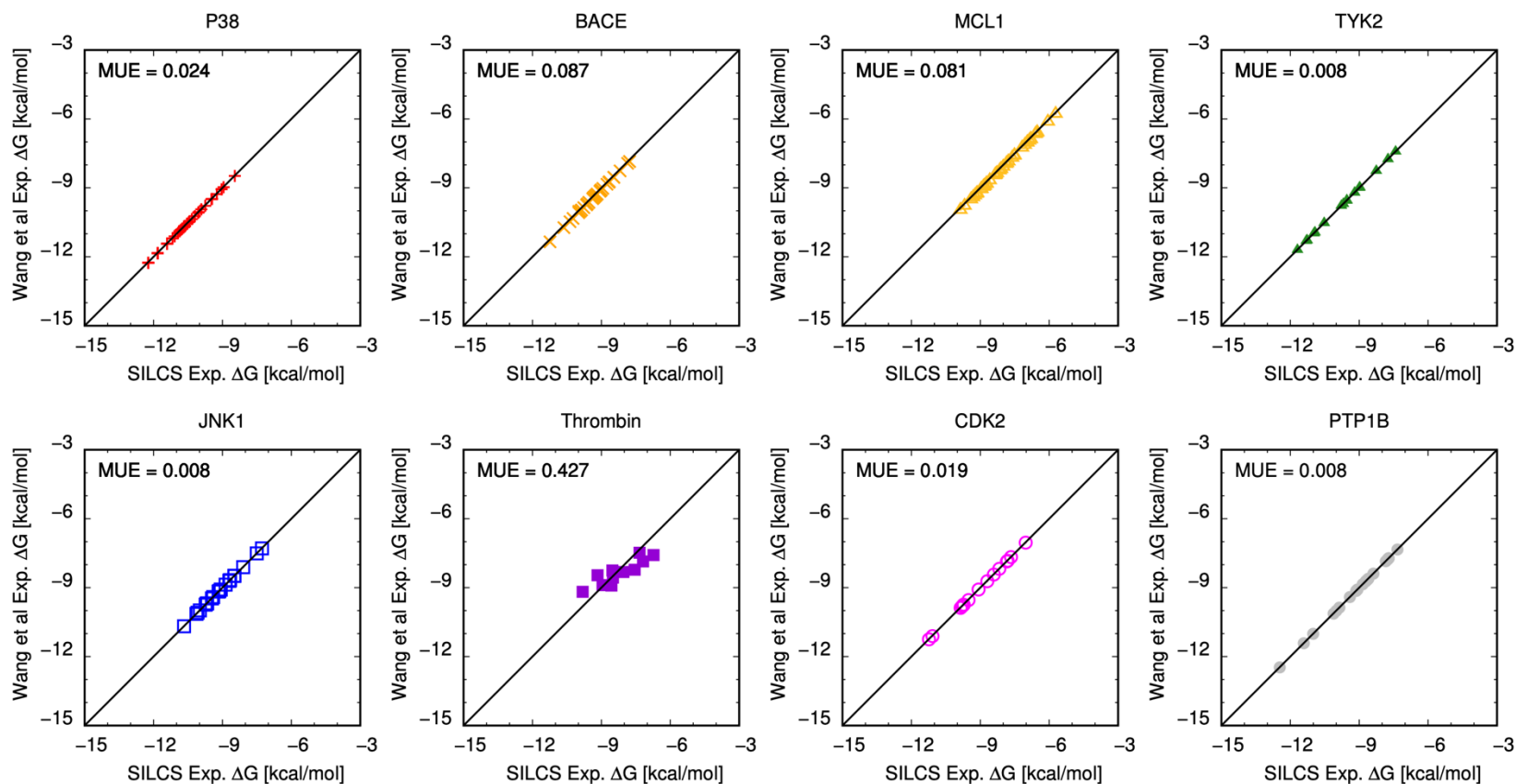


Figure S3: Experimental literature ΔG values reported in this work (SILCS) and from Wang et al.⁴ The MUE between the two sets of experimental numbers are indicated on the plots. All values show good agreement between this work and Wang et al.⁴ except for Thrombin. See SI section “Calculation of experimental binding free energies” for more details.

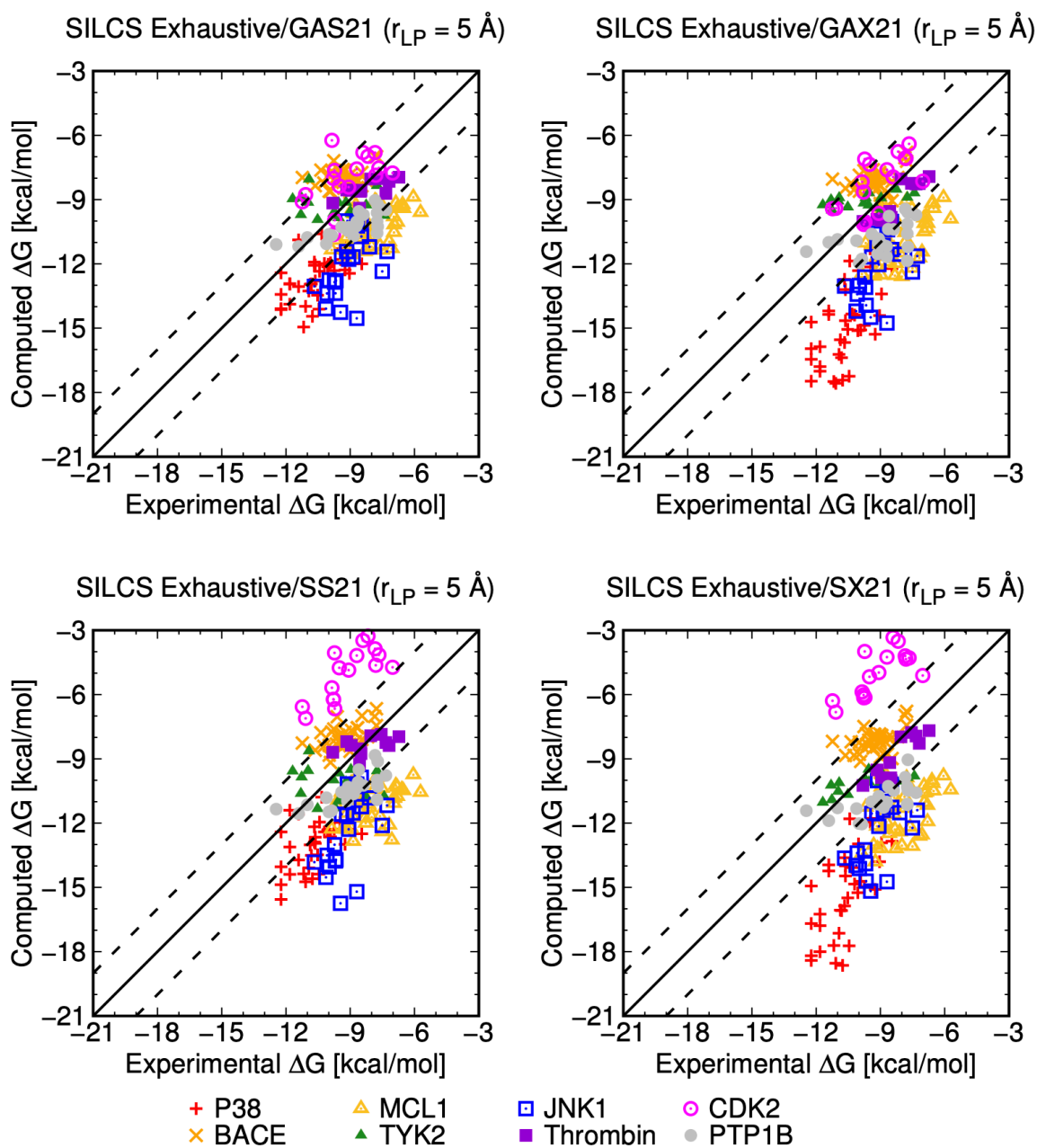


Figure S4: Raw LGFE scores vs experimental ΔG obtained from the GAS21, GAX21, SS21, and SX21 ACS with a 5 Å ligand placement radius for the 199 ligands. Dotted lines indicating error of ± 2 kcal/mol from the diagonal line.

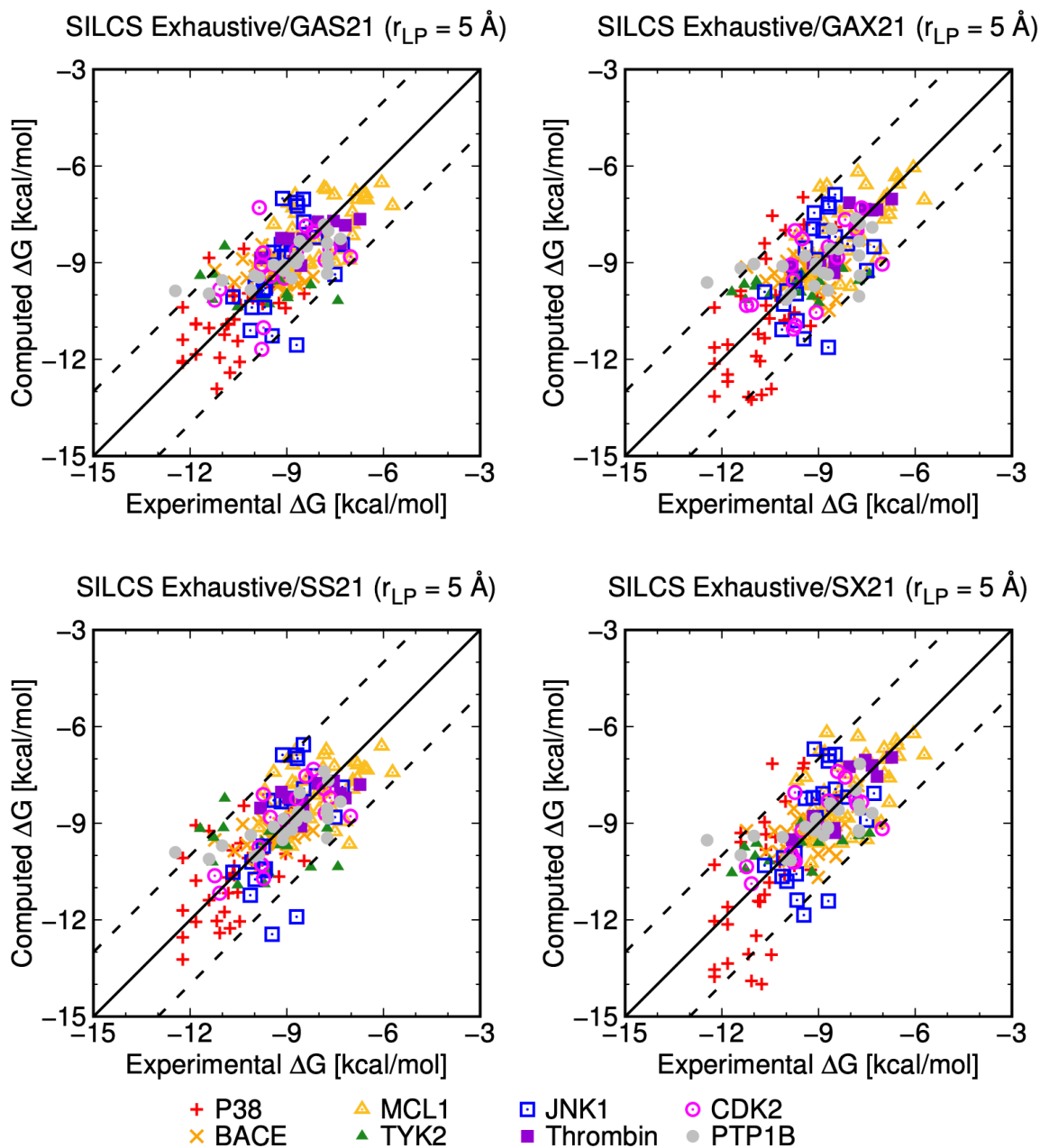


Figure S5: Computed versus experimental ΔG obtained from the GAS21, GAX21, SS21, and SX21 ACS with a 5 \AA ligand placement radius for the 199 ligands. Dotted lines indicating error of ± 2 kcal/mol from the diagonal line.

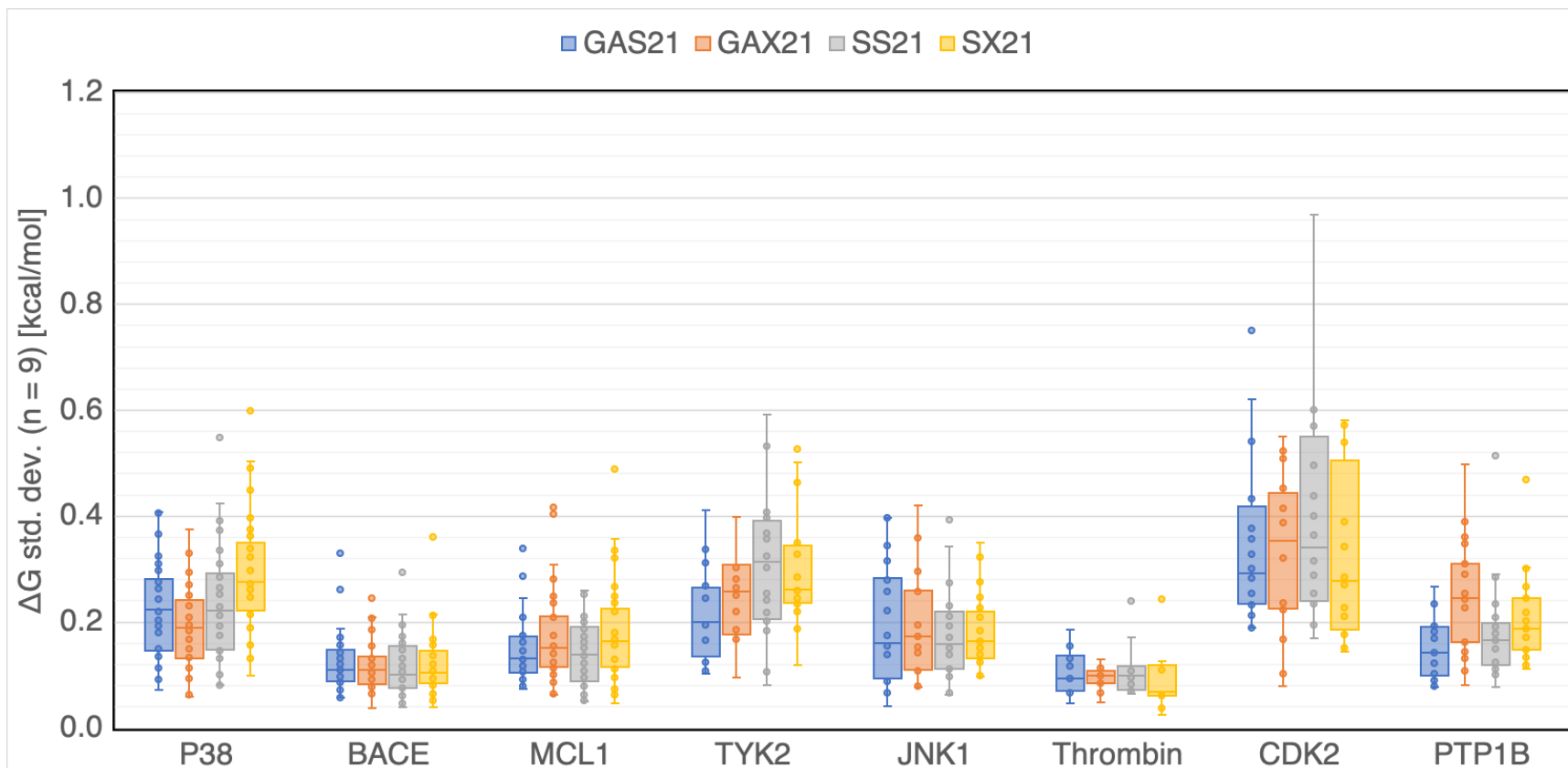


Figure S6: Standard deviations of binding free energies, ΔG , from $n = 9$ independent SILCS runs for individual ligands for each of the eight target proteins (ie. 199 total ligands). The box indicates the interquartile range (IQR), where the central 50% of all data points lie, with the center line indicating the median value. The whiskers extend out to $1.5 * \text{IQR}$. All individual data points are also plotted. All SILCS-MC runs were performed with a ligand placement radius of 5 \AA for all four ACS.

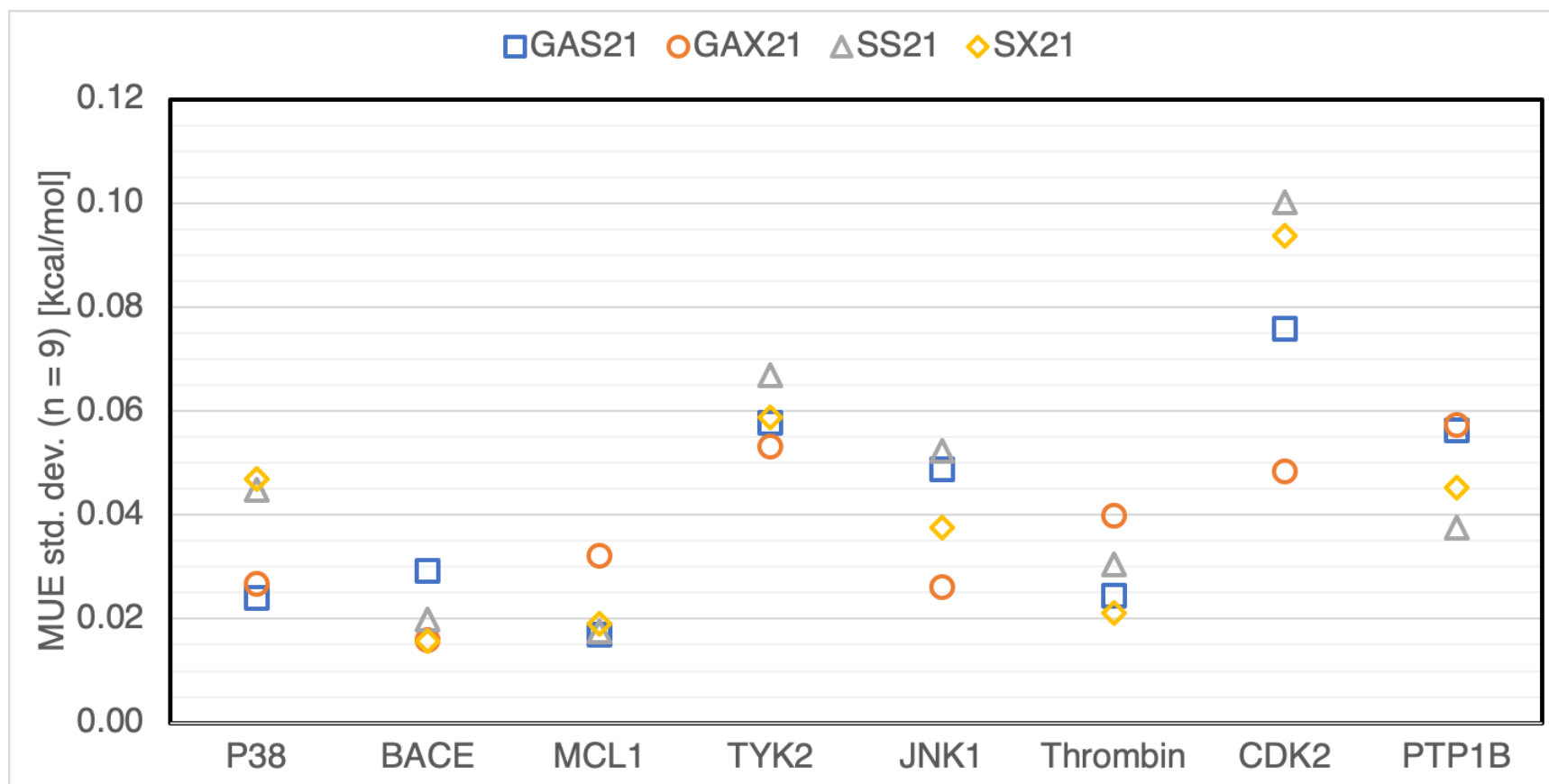


Figure S7: Standard deviations of MUE values calculated from $n = 9$ independent runs of the 199 ligands for the eight protein targets for all four ACS with a ligand placement radius of 5 Å.

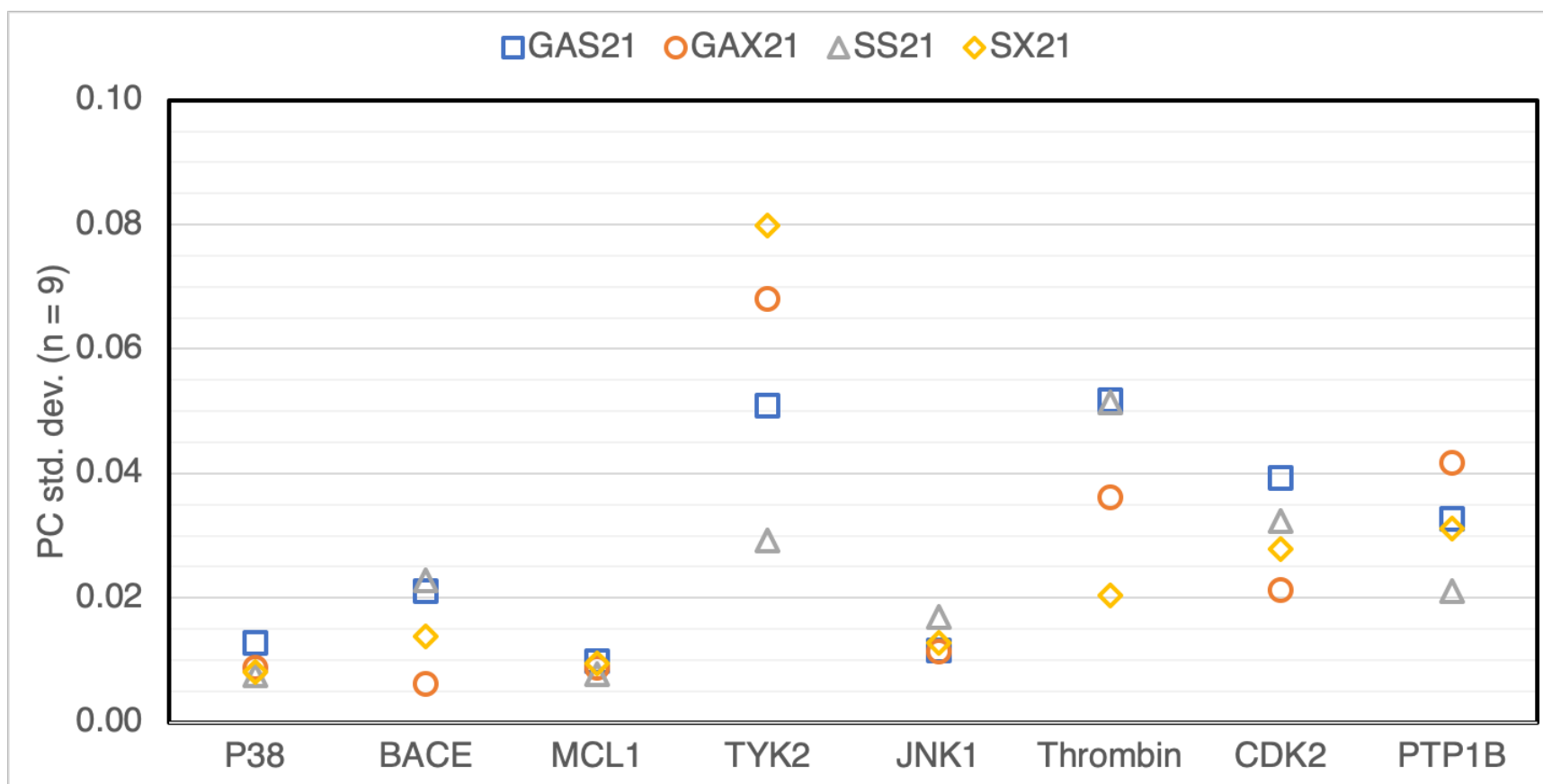


Figure S8: Standard deviations of PC values calculated from n = 9 independent runs of the 199 ligands for the eight protein targets for all four ACS models with a radius of 5 Å.

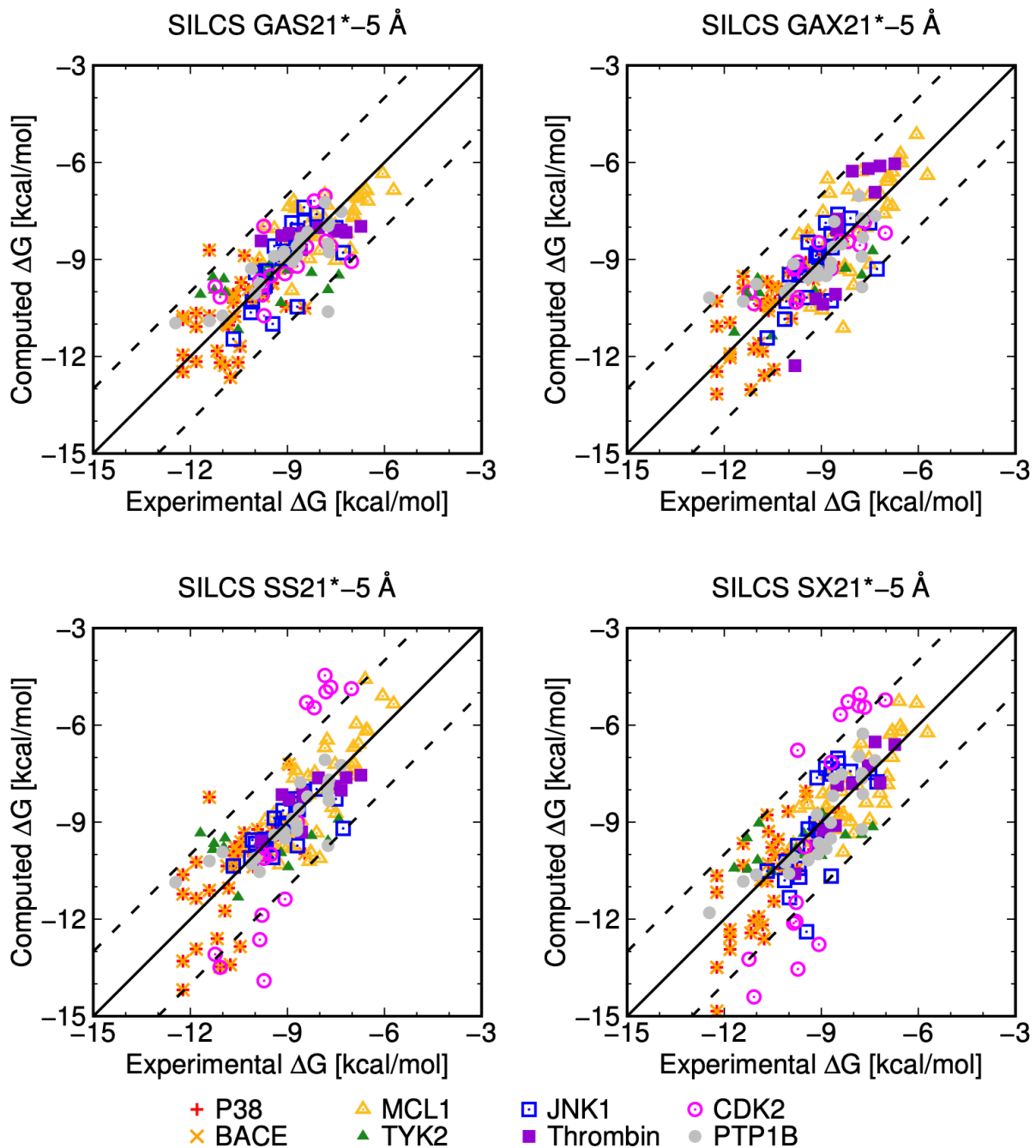


Figure S9: Computed versus experimental ΔG obtained from the PC-based ML optimization procedure for the 199 ligands using models GAS21, GAX21, SS21, and SX21 ACS with a ligand placement radius of 5 \AA .

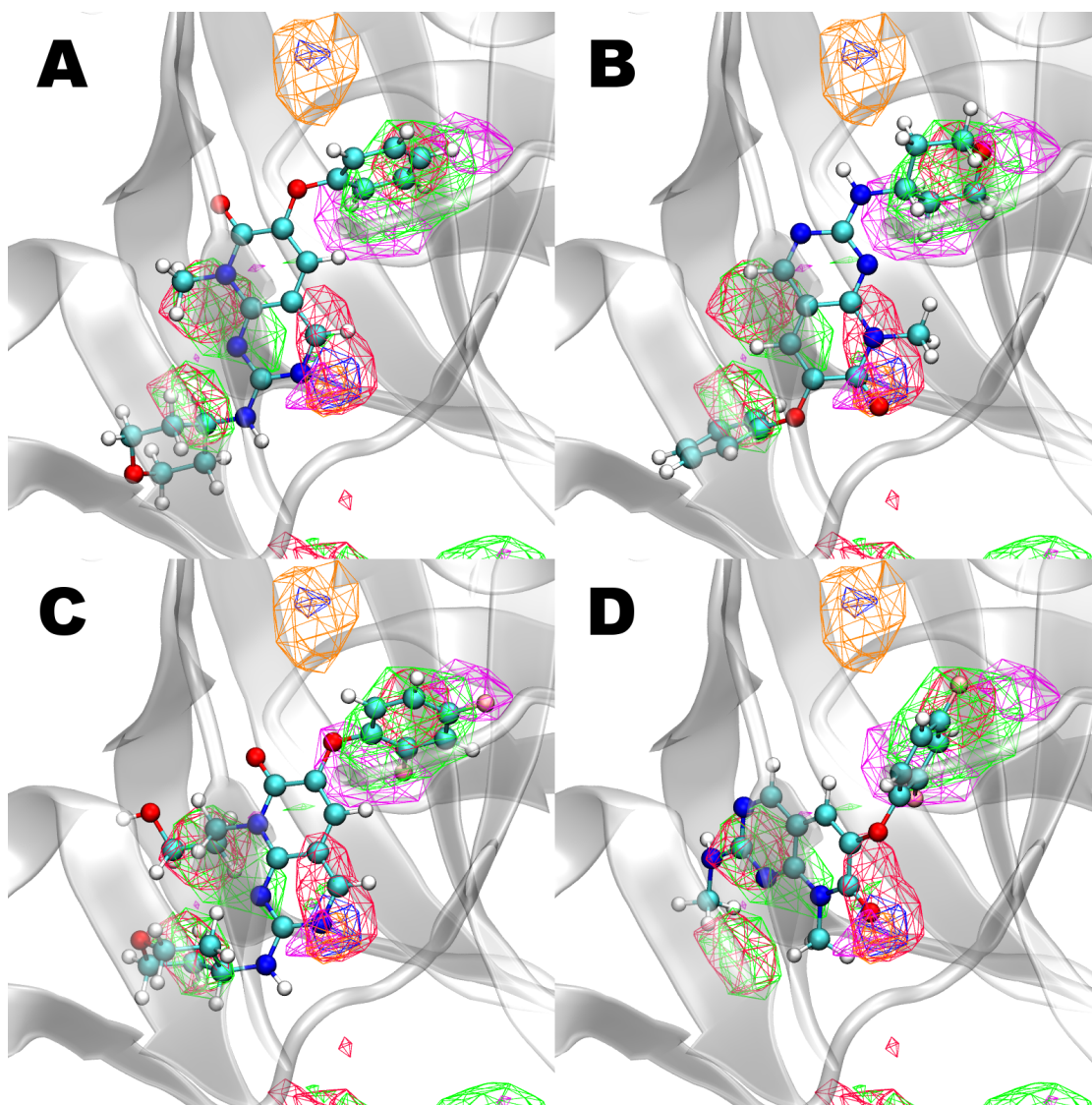


Figure S10: Outlier ligands for P38. Panels A, B, C, and D represent ligands 2d (crystal structure), 2d (SILCS pose), 2n (SILCS pose), and 2v (SILCS pose), respectively, within the binding pocket of P38. Ligand atoms are colored by element: (cyan) carbon, (red) oxygen, (blue) nitrogen, (pink) fluorine, and (white) hydrogen. Protein is shown in transparent cartoon representation. FragMaps are drawn for (green) generic apolar carbons, (red) dimethyl ether oxygen, (orange) formamide oxygen, (blue) imidazole acceptor nitrogen, and (magenta) fluorobenzene fluorine. Benzene and propane carbons are combined to produce the generic non-polar carbon maps. All FragMaps are drawn with an isocontour value of -1.2 kcal/mol. Experimental binding free energies and adjusted LGFE scores for ligands 2d, 2n, and 2v are -9.478 , -11.821 , and -8.948 kcal/mol and -7.187 , -13.858 , and -6.728 kcal/mol, respectively.

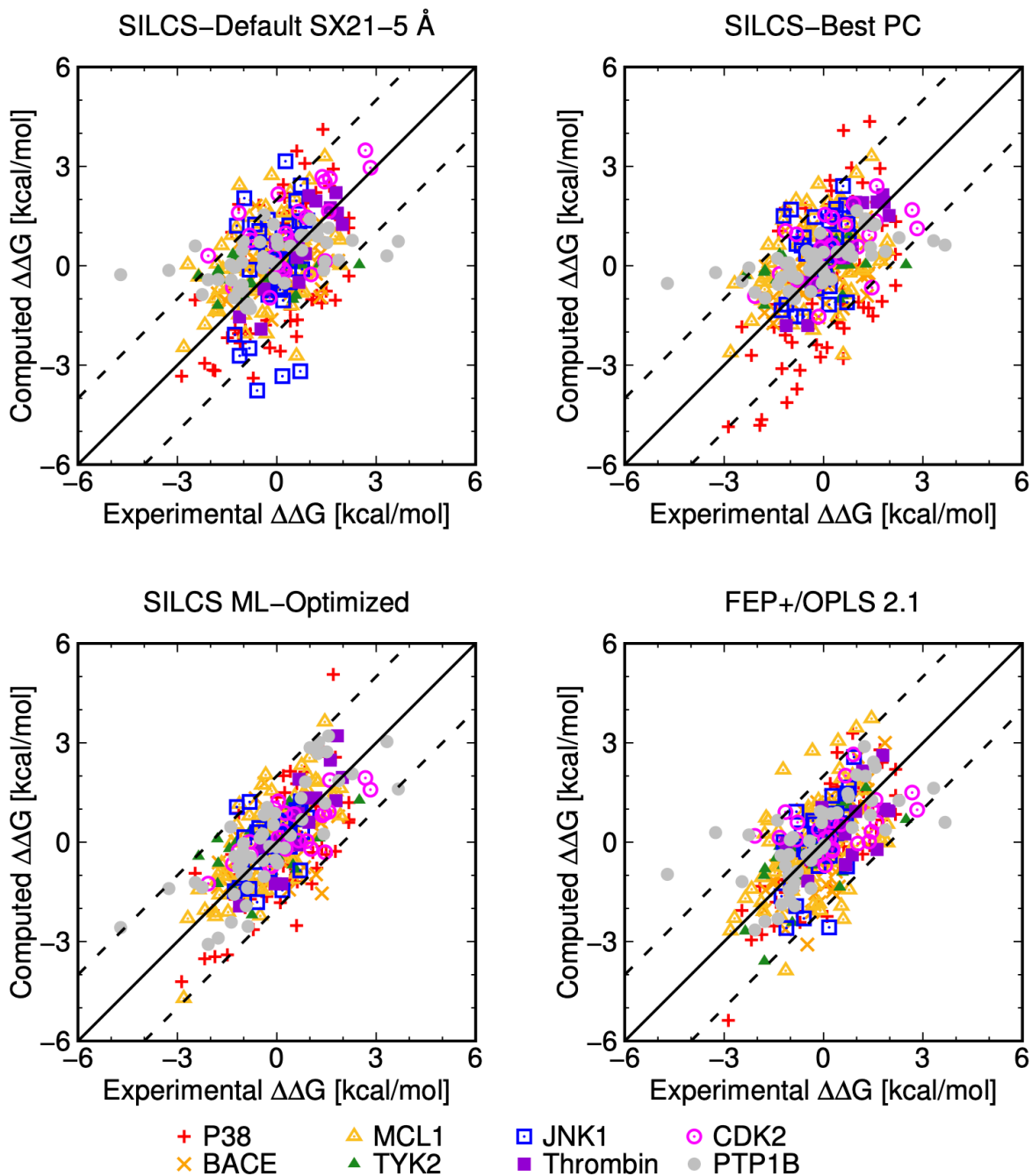


Figure S11: Computed versus experimental $\Delta\Delta G$ obtained from SILCS and FEP+/OPLS 2.1 for 330 perturbations between the 199 ligands.

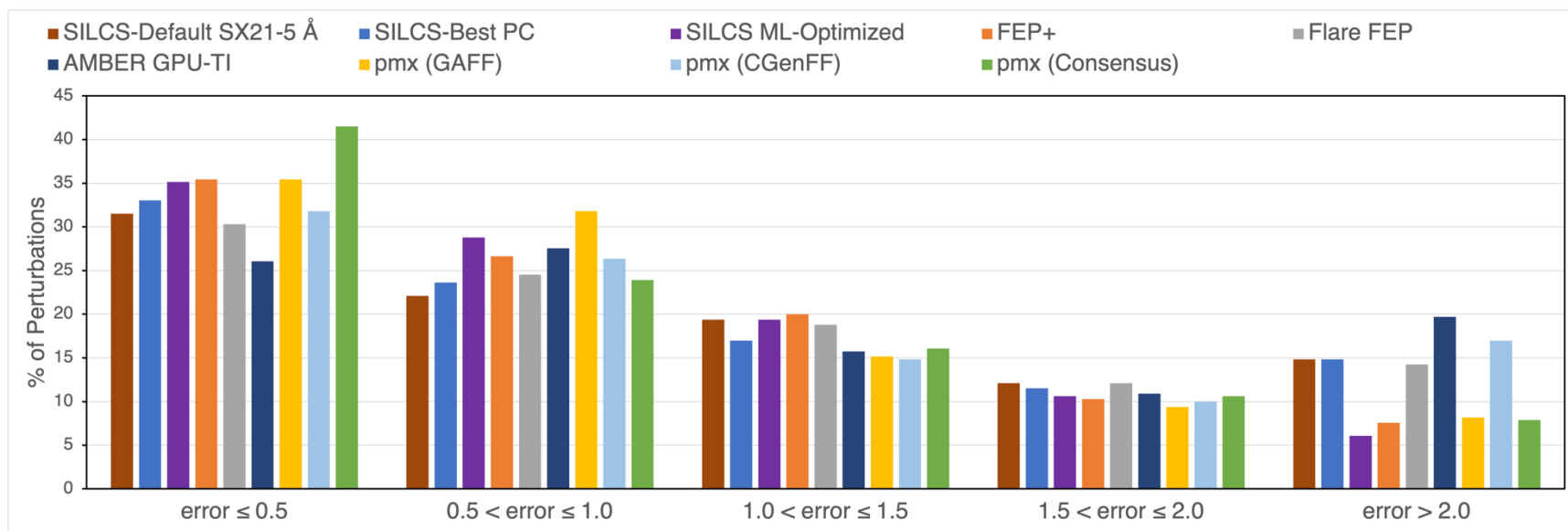


Figure S12: Percentage of ligand perturbations with $\Delta\Delta G$ unsigned error values (in kcal/mol) within the specified ranges for SILCS and other published data for 330 perturbations between 199 ligands.

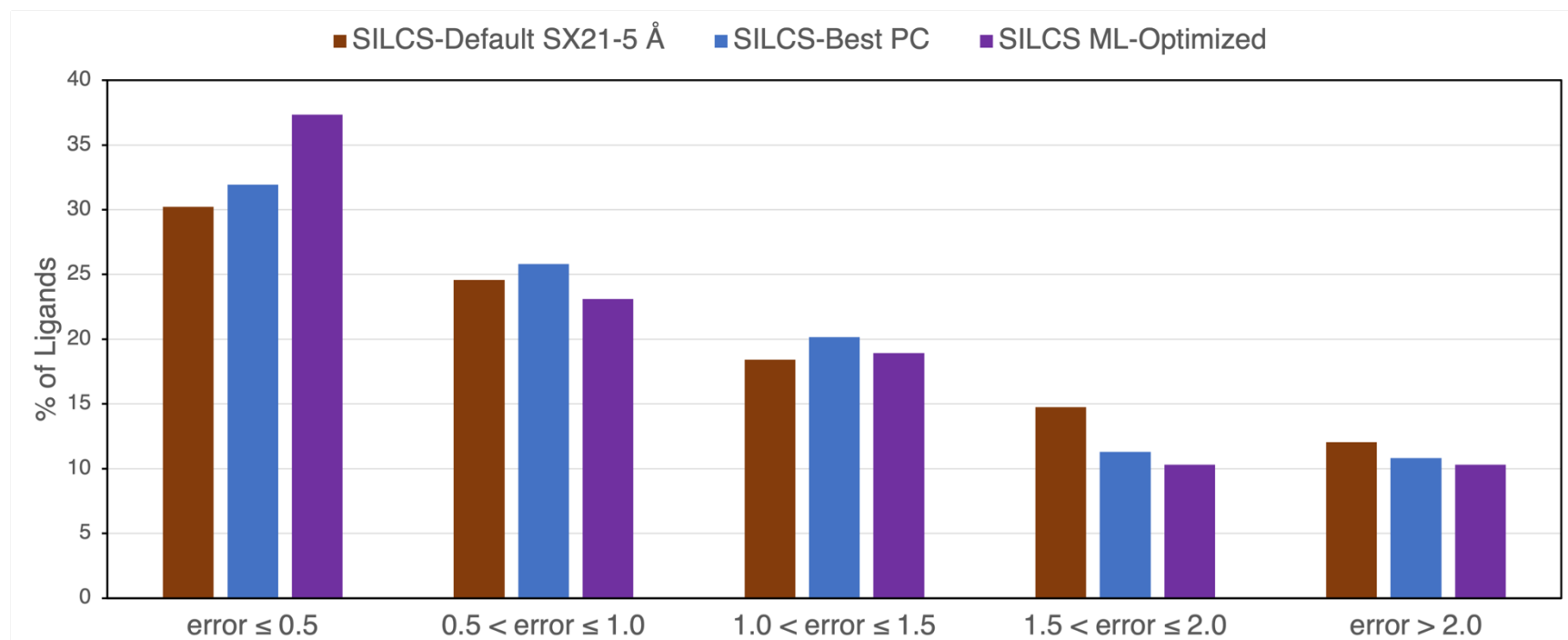


Figure S13: Percentage of ligands with ΔG unsigned error values (in kcal/mol) within the specified ranges for SILCS with 407 ligands.

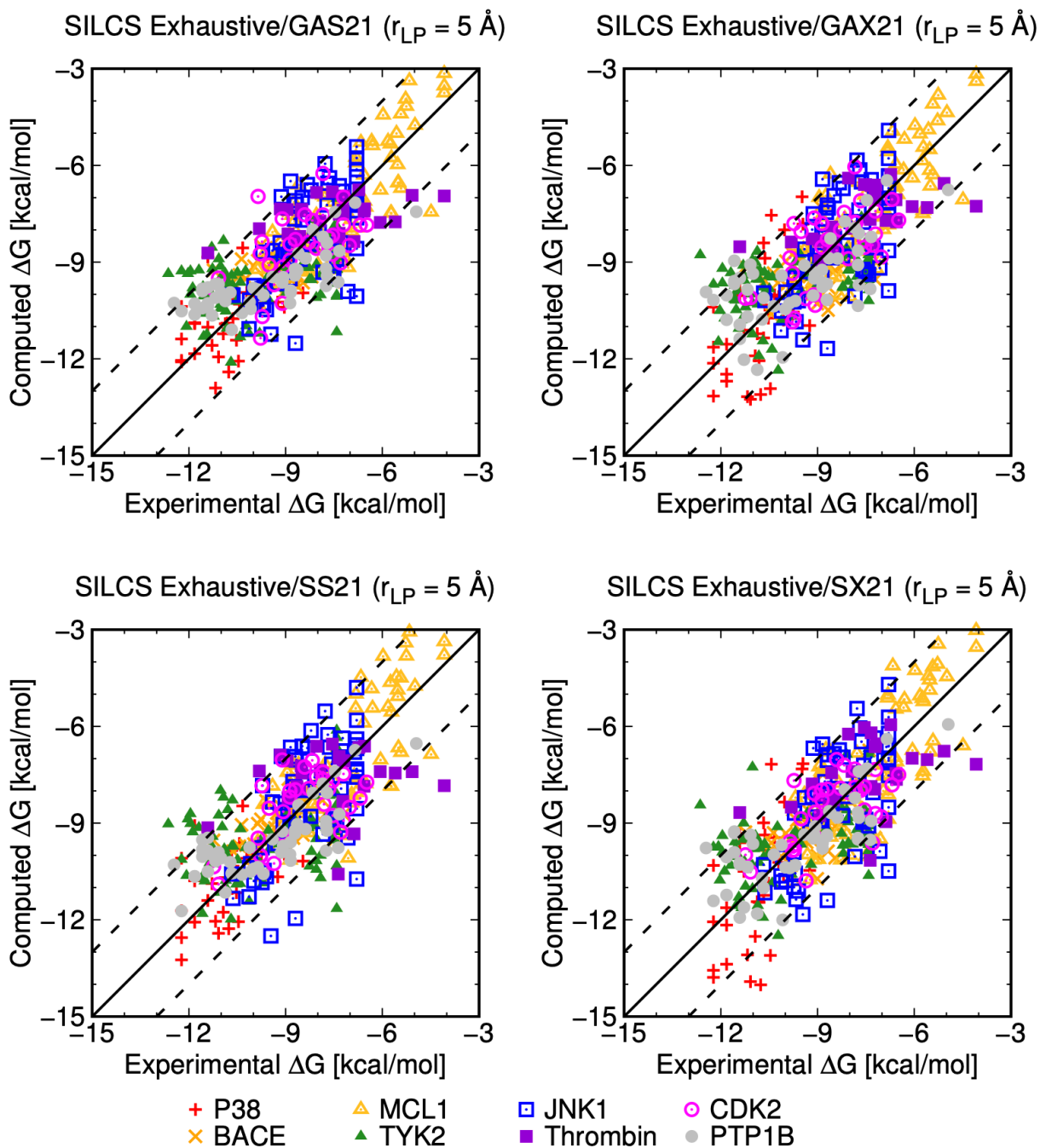


Figure S14: Computed versus experimental ΔG obtained from the GAS21, GAX21, SS21, and SX21 ACS with a ligand placement radius of 5 Å for the 407 ligands.

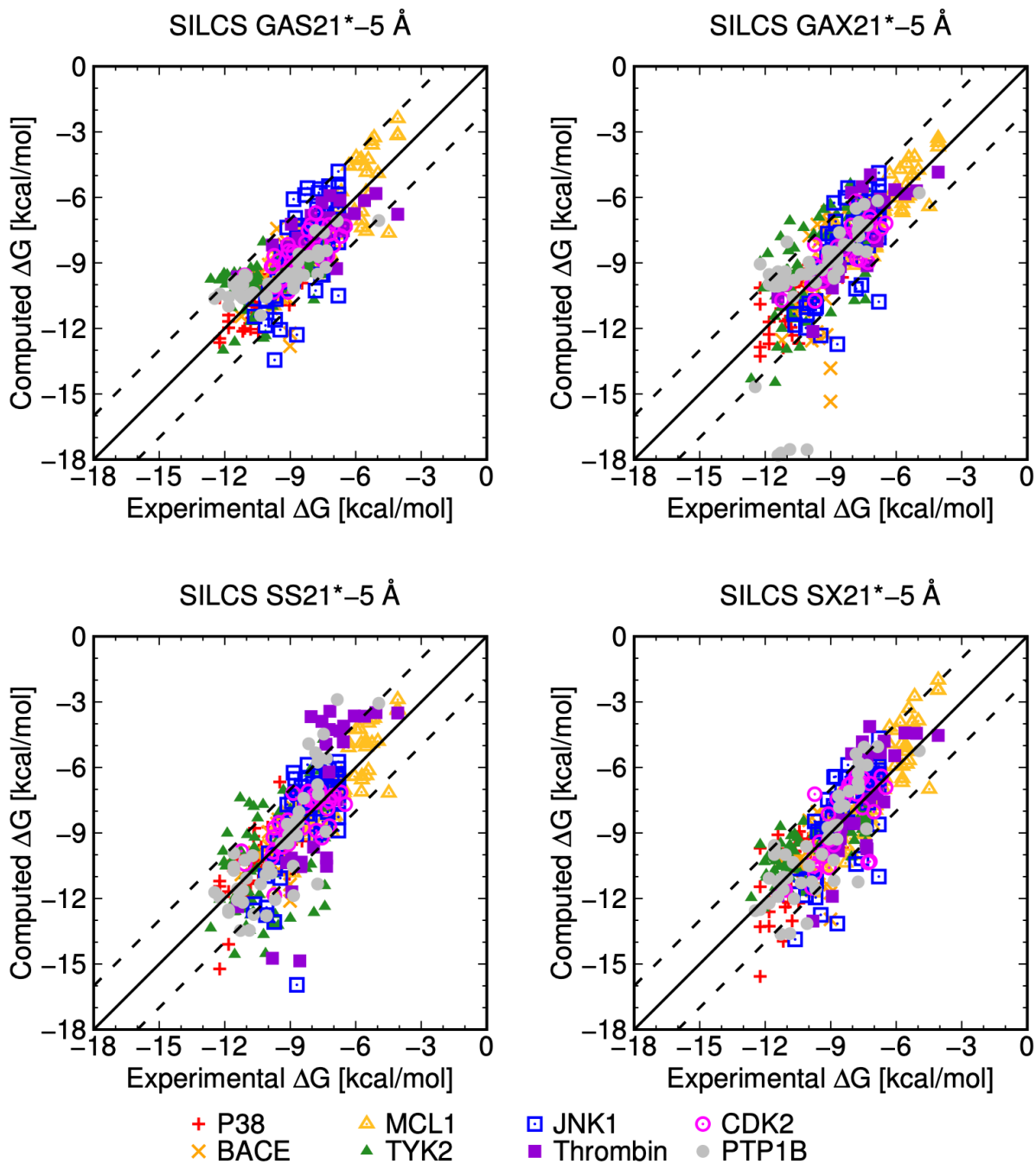


Figure S15: Computed versus experimental ΔG obtained from the PC-based ML optimization procedure for the 407 ligands using GAS21*, GAX21*, SS21*, and SX21* ACS with a ligand placement radius of 5 \AA .

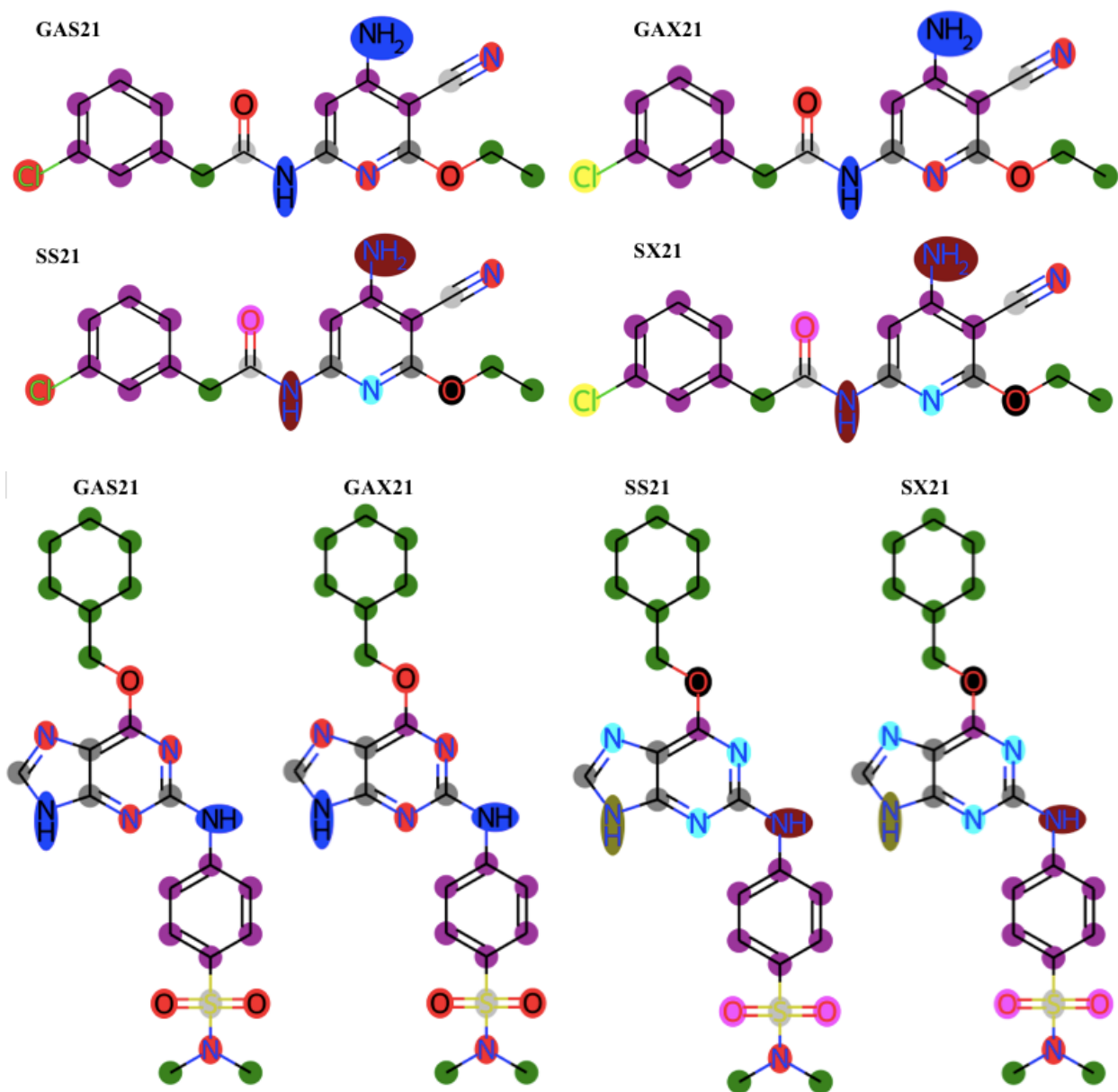


Figure S16: 2D chemical structure for the JNK1 (6g) and CDK2 (29) lead ligands with all Atom Classification Schemes. The atoms are colored based on the FragMap type for each non-hydrogen atom (see Table S1). The colors red, green, purple, blue, maroon, magenta, yellow, silver, gray, cyan, olive, and black represent GENA, PRPC, BENC, GEND, FORN, FORO, CLBx, NCLA, GEHC, IMIN, IMIH, and DMEO FragMap type, respectively. NCLA indicates non-classified atom type. All hydrogens are treated as NCLA.

References

1. V. D. Ustach, S. K. Lakkaraju, S. Jo, W. Yu, W. Jiang and A. D. MacKerell, Jr., *J. Chem. Inf. Model.*, 2019, **59**, 3018-3035.
2. E. P. Raman, W. Yu, O. Guvench and A. D. MacKerell, *J. Chem. Inf. Model.*, 2011, **51**, 877-896.
3. F. Y. Lin and A. D. MacKerell, Jr., *J. Phys. Chem. B*, 2017, **121**, 6813-6821.
4. L. Wang, Y. Wu, Y. Deng, B. Kim, L. Pierce, G. Krilov, D. Lupyan, S. Robinson, M. K. Dahlgren and J. Greenwood, *J. Am. Chem. Soc.*, 2015, **137**, 2695-2703.
5. B. Baum, M. Mohamed, M. Zayed, C. Gerlach, A. Heine, D. Hangauer and G. Klebe, *J. Mol. Biol.*, 2009, **390**, 56-69.
6. L. F. Song, T.-S. Lee, C. Zhu, D. M. York and K. M. Merz Jr, *J. Chem. Inf. Model.*, 2019, **59**, 3128-3135.
7. V. Gapsys, L. Pérez-Benito, M. Aldeghi, D. Seeliger, H. Van Vlijmen, G. Tresadern and B. L. de Groot, *Chem. Sci.*, 2020, **11**, 1140-1152.
8. M. Kuhn, S. Firth-Clark, P. Tosco, A. S. Mey, M. D. Mackey and J. Michel, *J. Chem. Inf. Model.*, 2020, **60**, 3120-3130.